# Low-Dimensional Structure in the Space of Language Representations is Reflected in Brain Responses

**Richard Antonello**
UT Austin
rjantonello@utexas.edu

**Javier Turek**
Intel Labs
javier.turek@intel.com

**Vy Vo**
Intel Labs
vy.vo@intel.com

**Alexander Huth**
UT Austin
huth@cs.utexas.edu

## Abstract

How related are the representations learned by neural language models, translation models, and language tagging tasks? We answer this question by adapting an encoder-decoder transfer learning method from computer vision to investigate the structure among 100 different feature spaces extracted from hidden representations of various networks trained on language tasks. This method reveals a low-dimensional structure where language models and translation models smoothly interpolate between word embeddings, syntactic and semantic tasks, and future word embeddings. We call this low-dimensional structure a *language representation embedding* because it encodes the relationships between representations needed to process language for a variety of NLP (natural language processing) tasks. We find that this representation embedding can predict how well each individual feature space maps to human brain responses to natural language stimuli recorded using fMRI. Additionally, we find that the principal dimension of this structure can be used to create a metric which highlights the brain's natural language processing hierarchy. This suggests that the embedding captures some part of the brain's natural language representation structure.

## 1 Introduction

There are a multitude of common techniques for analytically representing the information contained in natural language. At the word level, language is often represented by word embeddings, which capture some aspects of word meaning using word co-occurrence statistics [8, 25]. Language representations that highlight specific linguistic properties, such as parts-of-speech [29] or sentence chunks [1], or that utilize well-known NLP models such as the intermediate layers of pretrained language models [6, 10, 21, 27], are also frequently studied [12, 31]. In fields such as linguistics, natural language processing, and cognitive psychology, qualitative adjectives are often used to describe these language representations – e.g. "low-level" or "high-level" and "syntactic" or "semantic". The use of these words belies an unstated hypothesis about the nature of the space of language representations – namely that this space is fundamentally low-dimensional, and therefore that the information from the representations in this space can be efficiently described using a few categorical descriptors. In this work, we attempt to directly map the low-dimensional space of language representations by generating "representation embeddings" using a method inspired by the work of Zamir et al. [44]. This method uses the *transfer properties between representations* to map their relationships.

The work described here has two main contributions. First, we used the representation embeddings to demonstrate the existence of low-dimensional structure within the space of language representations.

35th Conference on Neural Information Processing Systems (NeurIPS 2021), Sydney, Australia.

We then used this structure to explore the relationships between – and gain deeper insight about – frequently used language representations. How do the intermediate layers of prominent language models relate to one another? How do the abstractions used by these layers evolve from low-level word embeddings of a context to a representation of the predicted next word for that context? Do different language models follow similar representation patterns? What are the differences between how unidirectional and bidirectional language models represent information? These are examples of the types of questions we can explore utilizing our representation embedding space. Second, we showed that this low-dimensional structure is reflected in brain responses predicted by these representation embeddings. In particular, we show that mapping the principal dimension of the representation embeddings onto the brain recovers, broadly, known language processing hierarchies. We also show that the representation embeddings can be used to predict which representations map well to each area in the brain.

## 2 Related Work

Our work closely follows the methods developed by Zamir et al. [44]. Those authors generated a taxonomy of vision tasks and analyzed their relationships in that space. This was achieved by applying transfer learning across vision tasks, and showed that this can reduce data labeling requirements. We used some of their methods, such as transfer modeling and normalization using analytic hierarchy process (AHP) [28], for our analysis on language tasks. Following the same lines but for NLP, the work from Vu et al. [37] explores transferability across NLP tasks. Those authors focus on the application of transfer learning to show that the amount of labeled data, source and target tasks, and domain similarity are all relevant factors for the quality of transferability. Kornblith et al. [20] investigated and compared techniques for measuring the similarity of neural network representations, such as canonical correlation analysis (CCA) and centered kernel alignment (CKA).

Our analysis of the relationship of between the language representation space and the brain leans heavily on the concept of "encoding models". Recently, encoding models have been widely applied as predictive models of brain responses to natural language [17, 40]. Jain and Huth [18] applied encoding models to representations of an LSTM language model that incorporates context into neural representations. These representations are explored for different timescales of language processing in Jain et al. [19]. Toneva and Wehbe [33] explored the encoding model performance of different language model layers to improve neural network performance. Caucheteux and King [5] observed differences in the convergence of hidden state representations from ANNs trained on various visual and language processing tasks to brain-like representations. Schrimpf et al. [30] systematically examined the performance of encoding models across a variety of representations and neural response datasets and observed consistent high performance of Transformer-based model hidden states at predicting neural responses to language. Wang et al. [39] constructed encoding models on a set of 21 vision tasks from Zamir et al. [44] with the objective of localizing tasks to specific brain regions. Those authors built a task graph of brain regions showing similar representation for highly transferable tasks.

## 3 Methods Overview

Our method aims to use the transfer properties between different language representations to generate quantitative descriptions of their relationships. These descriptions can then be used as an embedding space, without labelling any individual representation with predefined notions of what that representation is or how it relates to other representations. This is analogous to how word embeddings are generated by using co-occurrance statistics to generate quantitative descriptions of each word, without labelling any individual word with our predefined notions of what that word means. By using transfer properties to generate the embedding for each representation, we implicitly assume that language representations with similar transfer properties are themselves similar.

Formally, we define a *representation* $t$ as a function over a language input that extracts a vector of meaningful features for each word. Some representations can be computed independently for each word, such as word embeddings [1, 10, 25], while others depend on both a word and its context, such as part of speech labels [1], or the hidden state in some intermediate layer of a language model [5, 6, 27, 30]. We define a stimulus $\mathbf{s}$ as a string of words drawn from some natural language source, and $\mathcal{S}$ the set with all stimuli from that source. Our goal is to generate a representation embedding over a set of representations $\mathcal{T}$ that are derivable from the same stimuli $\mathcal{S}$. That is, for a

representation $t \in \mathcal{T}$, and for all times $j$ in our stimulus $\mathbf{s} \in \mathcal{S}$, $t(\mathbf{s}_j)$ is defined. By extension, there is a natural time-dependent mapping between representations, as for each pair of representations $t_1, t_2 \in \mathcal{T}$ for identical times, we can attempt to map $t_1(\mathbf{s}_j)$ to $t_2(\mathbf{s}_j)$. This provides a standardized transfer mapping $f_{t_1 \to t_2}(\cdot)$ that can be learned for each pair of representations,

$$f_{t_1 \to t_2}(t_1(\mathbf{s}_j)) \approx t_2(\mathbf{s}_j) \qquad \forall j.$$

However, learning these transfer mappings directly would make comparison across representations difficult, as many of the representations have different dimensionalities. Instead, we adapted the encoder-decoder framework proposed in Zamir et al. [44], which ensures that every transfer mapping has the same input dimensionality. This method proceeds in three parts (Figure 1):

First, we train a linear encoder for each representation that compresses the information in the input down into a latent space. The latent space should only contain information necessary to predict the given representation's features from our input. This is accomplished by training an encoder-decoder from the input to the given representation via a latent space, then discarding the decoder.

Second, we train a new decoder for each pair of representations that uses the previously generated latent space for one representation to predict the other representation.

Third, we evaluate the performance of each decoder targeting a given representation relative to every other decoder for that same representation. This provides a measure of how much of the information in one representation is present in each other representation. Just as words that have similar co-occurrence statistics–when measured against a large enough group of other words–are thought to have similar meanings, we argue that pairs of representations that have similar transfer properties–when measured against a large enough group of other representations–have similar information content.

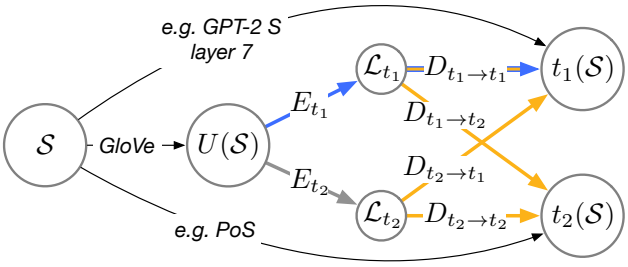


Figure 1: The encoder-decoder setup of our method, adapted from Zamir et al. [44]. $\mathcal{S}$ is our natural language story stimuli. This can be represented by in many ways, including by our universal input feature space $U(\mathcal{S})$, which were GloVe word embeddings. Encoders $E_{t_i}$ were trained using a bottlenecked linear encoder-decoder network, which outputs to $t_i(\mathcal{S})$ (*blue arrows*). The decoding half of this network was then discarded, and the encoding half used to generate a latent space $\mathcal{L}_{t_i}$ for each representation $t_i$. Then, a decoder is trained from each latent space to each representation (*orange arrows*). The performance of decoders that map to the same final representation are then compared to one another.

### 3.1 Generating Representation Encoders

We define[1] $U(\mathcal{S})$ as the universal input feature space for our stimuli $\mathcal{S}$. In practice, this space should represent the input with high fidelity, so could be selected as a one-hot encoding of each input token, or word embeddings for each input token. We use GloVe word embeddings for $U(\mathcal{S})$. Now let $\mathcal{T}$ be a set of representations over $\mathcal{S}$. For each representation $t \in \mathcal{T}$, we generate an encoder $E_t(\cdot)$ such that the encoder extracts only information in $U(\mathcal{S})$ that is needed to predict $t(\mathcal{S})$. We do this by using a bottlenecked linear neural network that maps every $\mathbf{u} \in U(\mathcal{S})$ to an intermediate low-dimensional latent space $\mathcal{L}_t = E_t(U(\mathcal{S}))$ and then maps it to the given representation space,

$$t(\mathbf{s}) \approx f(E_t(\mathbf{u})) \qquad \forall \mathbf{s} \in \mathcal{S} \wedge \mathbf{u} = U(\mathbf{s}),$$

where $f(\cdot)$ is mapping from $\mathcal{L}_t$ to $t(\mathcal{S})$. We used a small latent space of 20 dimensions to encourage the encoder to extract only the information in $U(\mathcal{S})$ that is relevant to compute $t(\mathcal{S})$. Experimentation

[1] We assume that elements $j$ in a string $\mathbf{s}_j$ are properly treated, such that we can exclude the positional indexes for all $\mathbf{s}$. Thus, we define $U(\mathcal{S}) = \{U(\mathbf{s}) | \mathbf{s} \in \mathcal{S}\}$ as the result of applying a function $U(\cdot)$ to all elements $s \in \mathcal{S}$.

showed that variations in the latent space size do not meaningfully change encoder performance. Once we have learned these mappings, we assign $E_t$ to be our representation encoder for each representation $t \in \mathcal{T}$. Regardless of the dimensionality of the representation, each latent space has a fixed dimensionality, which enables a fair comparison between representations.

### 3.2 Generating Representation Decoders

The encoders for each representation generate a latent space $\mathcal{L}_t$ that extracts the information in $U(\mathcal{S})$ relevant to computing $t(\mathcal{S})$, while compressing away irrelevant information. For every pair of representations $(t_1, t_2) \in \mathcal{T}$, we next generate a decoder $D_{t_1 \to t_2}$ such that $D_{t_1 \to t_2}(\mathcal{L}_{t_1}) = D_{t_1 \to t_2}(E_{t_1}(U(\mathcal{S})))$ approximates $t_2(\mathcal{S})$. This yields a total of $n^2$ decoders, where $|\mathcal{T}| = n$ is the total number of representations. All networks were trained with batches of size 1024 and standard stochastic gradient descent with a learning rate of $10^{-4}$ for the initial encoders and $2 \times 10^{-5}$ for the decoders. Hyperparameters were chosen via coordinate descent.

### 3.3 Generating the Representation Embedding Matrix

Finally, we compare the performance of the $n$ decoders for each representation in order to generate the representation embedding space. To ensure that comparisons are made on equal footing, we only compare decoders with the same output representation (e.g. $D_{t_1 \to t_2}$ is compared with $D_{t_3 \to t_2}$, $D_{t_4 \to t_2}$, etc.). Further, we should consider that evaluating representations in with varying dimensions would yield results in different scales. Therefore, this requires normalizing all values. This and other challenges were pointed out by Zamir et al. [44].

Specifically, we generate a pairwise *tournament matrix* $\mathbf{W}_t$ for each representation $t$ by "fighting" all pairs of decoders that output to representation $t$ using a held-out test set $\mathcal{S}_{test}$ of sentences. Namely, element $(i, j)$ in $\mathbf{W}_t$ contains the ratio of samples in the test set that $D_{t_i \to t}$ has lower MSE than $D_{t_j \to t}$, i.e., $\mathbf{W}_{t_{(i,j)}} = \frac{\mathbb{E}_{\mathbf{s} \in \mathcal{S}_{test}}\left[D_{t_i \to t}(\mathbf{s}) < D_{t_j \to t}(\mathbf{s})\right]}{\mathbb{E}_{\mathbf{s} \in \mathcal{S}_{test}}\left[D_{t_j \to t}(\mathbf{s}) < D_{t_i \to t}(\mathbf{s})\right]}$. For example, if the decoder $D_{A \to C}$ has lower mean squared error than decoder $D_{B \to C}$ for 75% of the data in $\mathcal{S}_{test}$, we assign the ratio of $0.75/0.25 = 3$ to the triplet of representations $(A, B, C)$. This value would be stored in entry $(A, B)$ in the tournament matrix $\mathbf{W}_C$ for representation $C$.

We then use this set of pairwise comparisons to approximate a total order over the quality of all encoders for each decoded representation. We do this using a technique called the Analytic Hierarchy Process (AHP) [28], a technique commonly used in operations research to convert many pairwise comparisons into an estimated total order. AHP establishes that the elements of the principal eigenvector of $\mathbf{W}_t$ constitutes a good candidate for a total order over the encoders for $t$. This eigenvector is proportional to the time that an infinite length random walk on the weighted bidirected graph induced by $\mathbf{W}_t$ will spend at any given representation. Thus, if the encoder for one representation is better than the others, the weight on that representation will be higher as compared to the weights of other encoders. This eigenvector is then normalized to sum to 1. This procedure yields a length $n$ vector for each of the $n$ representations. We set a value of $0.1$ into each vector at the position corresponding to the target representation, and then stack the resulting length $n$ vectors together into the representation embedding matrix, $\mathbf{R}$. [2]

## 4 Results

### 4.1 Language Representation Embeddings

We applied our method to a set of 100 language representations taken from precomputed word embeddings or pretrained neural networks for NLP tasks operating on English language inputs. We extracted representations from numerous different tasks, which included three word embedding spaces (GloVe, BERT-E, FLAIR) [25, 10, 1], three unidirectional language models (GPT-2 Small, GPT-2 Medium, Transformer-XL) [27, 6, 41], two masked bidirectional language models (BERT, ALBERT) [10, 21], four common interpretable language tagging tasks (named entity recognition, part-of-speech identification, sentence chunking, frame semantic parsing) [1], and two machine translation models (English $\to$ Mandarin, English $\to$ German) [32]. We also included the GloVe embedding for the next word in the sequence, which constitutes a low-dimensional representation of the ideal output

[2] Data and open-source demonstration code that implements the methods and some results from this paper is available at `https://github.com/HuthLab/rep_structure`.

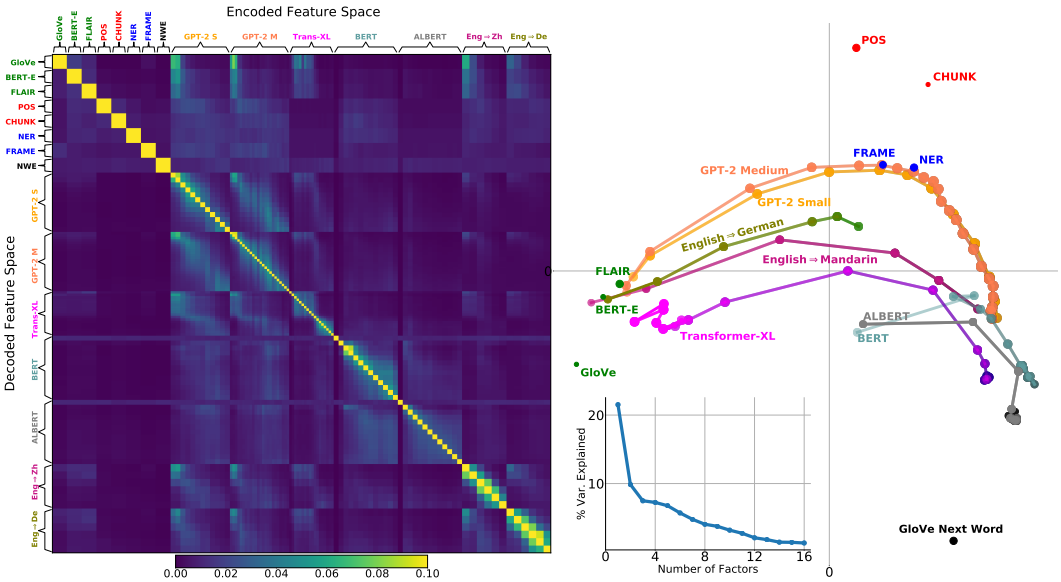


Figure 2: *Language Representation Embeddings with Low Dimensionality:* (*Left*): The representation embedding matrix $\mathbf{R}$ shows how well a given linguistic feature space (encoder, columns) transfers to another feature space (decoder, rows). For better visualization, rows and columns corresponding to different layers from the same network have been scaled down in this plot. A full-scale matrix is in the supplementary material. (*Right*): Applying multi-dimensional scaling to the representation embedding matrix reveals low-dimensional structure in the linguistic feature spaces. It is dominated by a left-to-right progression from the input word embedding, to syntactic and semantic tagging tasks near the middle layers of language models, to the next word embedding. Multidimensional scaling was weighted such that each full model had equal weight, ensuring that models were not more influential on account of having more layers. The dominant main diagonal was set to 0.1 to preserve the effects of off-diagonal values. The scree plot in the lower left shows that these first two dimensions explain substantially more variance (22% and 10%) than other dimensions, demonstrating that the structure in this space is low-dimensional. The size of each marker indicates the performance of that representation as an encoding model.

of a language model. For multilayered networks (language and translation models), we extracted all intermediate layers as separate representations. Full descriptions of all representations, as well as details on how each feature space is extracted, can be found in Appendix A.

Applying our method to these representations, we generated a representation embedding space (Figure 2). Generating this space took roughly one week of compute time on a cluster of 53 GPUs (a combination of Titan X, Titan V, and Quadro RTXs) and 64 CPU servers of different characteristics (Intel[3] Broadwell, Skylake, and Cascade Lake). The representations were trained on a text corpus of stories from *The Moth Radio Hour* [36] which totalled approximately 54,000 words. The held-out test set for the tournament matrix included a story of 1,839 words. Each row shows the relative performance of each of the 99 other representations in decoding a given representation. Each column shows how well a given encoded representation can decode to the other representations. Note that there is a distinct asymmetry: if a given representation (e.g. part-of-speech tagging) is never the best encoder for any other representation, then its column will contain very low values. However, other representations may decode to this one quite well, so the corresponding part-of-speech row can contain higher values.

### 4.1.1 Multidimensional Scaling Analysis

To better visualize the relationships between the representations, we performed multidimensional scaling (MDS) [34] on the rows of the representation embedding matrix. We then plotted the representations according to their locations on the first two MDS dimensions (Figure 2). This showed that the layers of each of the unidirectional language models form similar trajectories through the

[3]Intel, the Intel logo, and other Intel marks are trademarks of Intel Corporation or its subsidiaries. Other names and brands may be claimed as the property of others.

space, beginning near the word embeddings (*green*) and ending relatively close to the next-word embedding (*black*). This trajectory is monotonic on the first MDS dimension, but values on the second MDS dimension rise and then fall, with the highest values assigned to the middle layers (e.g. layer 5 of 12 in GPT-2 small). Language tagging tasks that require semantic information, such as framing and named entity recognition (*blue*), are close in space to the middle layers of the unidirectional language models. Language tagging tasks that required syntactic information, such as part-of-speech identification and sentence chunking (*red*), are similarly clustered.

We also observe several other interesting relationships. The machine translation representations also begin near the word embeddings. However, translation to Mandarin (Eng→Zh) appears to align more closely to fairly deep layers of the unidirectional language models, compared to translating from English to German. This may be because English and Mandarin are less closely related to one another, and could require deeper syntactic and semantic processing for successful translation.

We also observe that the bidirectional language model representations begin farther away from the input word embedding, closer to the middle of the unidirectional language models. However, they do also end up in a similar point, closer to the next-word embedding. This may be a result of the procedure to extract a feature space from the intermediate layers of the bidirectional language models, which differed meaningfully from extracting the intermediate layers of the unidirectional language models. Since these networks are trained on a masked language modeling task, we extracted the hidden representation for the token immediately preceding the mask token.

To study the dimensionality of the space of language representations, we examined the variance explained by low-dimensional approximations of the embedding matrix. The scree plot in Figure 2 shows the result of applying exploratory factor analysis (EFA) [43] to the representation embedding matrix. We see that the first few dimensions explain much more variance in the matrix than the other dimensions. The first dimension alone constitutes a full 22% of variance. This demonstrates that the representation embedding matrix–and thus, we infer, the space of language representations–has low-dimensional structure.

### 4.2 Representation Embeddings Predict fMRI Encoding Model Performance

Next, we hypothesized that these language representation embeddings are a useful representation of how natural language is processed in the human brain. Since it is the only system truly capable of producing and understanding complex language, the human brain is an excellent litmus test to determine whether this low-dimensional embedding captures the underlying structure of linguistic information. To test this hypothesis, we used the representation embeddings generated above to predict how well each representation is able to predict fMRI data collected from the human brain as the subject is listening to natural language stories.

#### 4.2.1 fMRI Data

We used functional magnetic resonance imaging (fMRI) data collected from 5 human subjects as they listened to English language podcast stories over Sensimetrics S14 headphones. Subjects were not asked to make any responses, but simply to listen attentively to the stories. For encoding model training, each subject listened to at approximately 5 hours of unique stories across 5 scanning sessions, yielding a total of 9,189 datapoints for each voxel across the whole brain. For model testing, the subjects listened to the same test story once in each session (i.e. 5 times). These responses were then averaged across repetitions. Training and test stimuli are listed in Appendix B.1. Functional signal-to-noise ratios in each voxel were assessed by applying the mean-explainable variance method from Nishimoto et al. [24] to the repeated test data. Only voxels within 8 mm of the mid-cortical surface were analyzed, yielding roughly 90,000 voxels per subject.

MRI data were collected on a 3T Siemens Skyra scanner at the University of Texas at Austin Biomedical Imaging Center using a 64-channel Siemens volume coil. Functional scans were collected using a gradient echo EPI sequence with repetition time (TR) = 2.00 s, echo time (TE) = 30.8 ms, flip angle = 71°, multi-band factor (simultaneous multi-slice) = 2, voxel size = 2.6mm x 2.6mm x 2.6mm (slice thickness = 2.6mm), matrix size = 84x84, and field of view = 220 mm. Anatomical data were collected using a T1-weighted multi-echo MP-RAGE sequence with voxel size = 1mm x 1mm x 1mm following the Freesurfer [15] morphometry protocol.

Experiments were approved by the University of Texas at Austin IRB. All subjects gave written informed consent. Subjects were compensated for their time at a rate of $25 per hour, or $262 for the entire experiment. Compensation for the 5 subjects totaled $1260.

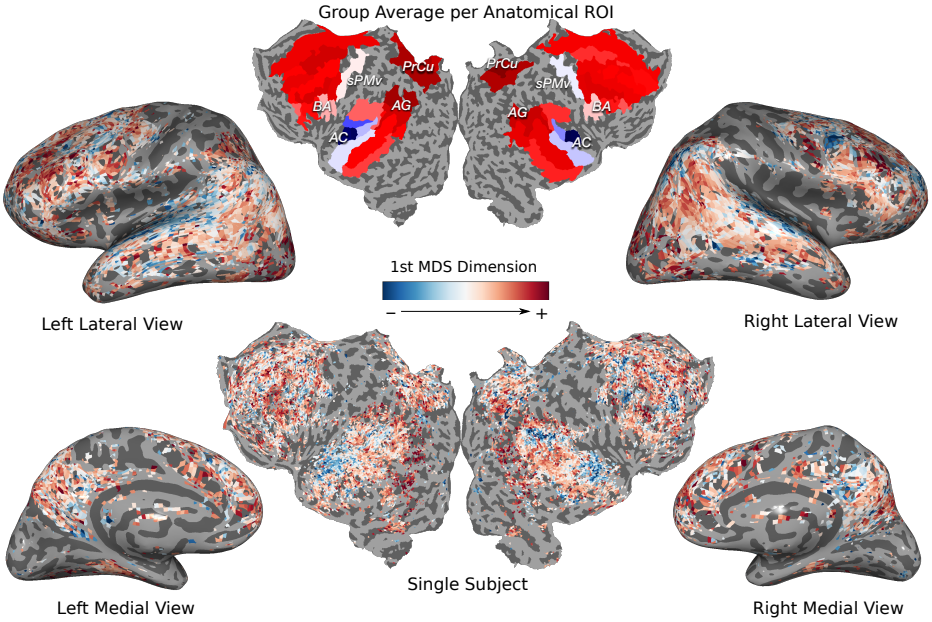


Figure 3: *Embedding Brain Voxels in the first MDS dimension:* Projection of the encoding performance vectors for each voxel in one subject (*lower center*) and averaged over all subjects and across regions (*upper center*) over the 100 representations onto the first MDS dimension of the representation embeddings, which explains about 20% of the variance in the representation embeddings. Voxels with high values in this embedding (*red*) are well-explained by representations that are more positive on the main MDS dimension (e.g. later language model layers), and voxels with low values (*blue*) are explained by representations that are more negative (e.g. word embeddings). This dimension is notable as it is the main dimension along which language representations evolve from "earlier" representations such as word embeddings, to "later" representations such as intermediate layers in deep language models. Anatomical ROIs were defined automatically in each subject using Freesurfer with the Destrieux 2009 atlas [9]. Similar maps for the other subjects and a plot showing the numerical projection of regions in the MDS space are shown in Appendix D.1.

#### 4.2.2 fMRI Encoding Models

Encoding models predict a measured brain response $B$, e.g. blood-oxygen-level dependent (BOLD) responses recorded with fMRI, based on the stimulus observed by the subject. Due to limitations on dataset size, encoding models are typically structured as linearized regression, where each regression predictor is some feature of the stimulus. Encoding models can provide insight into where and how information is represented in the brain. For instance, an encoding model that has a feature for whether a given auditory stimulus is a person's name can be used to determine which regions of the brain are activated by hearing names.

Here we constructed voxelwise encoding models using ridge regression for each of the 100 language representations $t$ analyzed above. Let $g(t_i)$ indicate a linearized ridge regression model that uses a temporally transformed version of the representation $t_i$ as predictors in the regression. The temporal transformation accounts for the lag in the hemodynamic response function [23]. We use time delays of 2, 4, 6, and 8 seconds of the representation to generate this temporal transformation. For each subject $x$, voxel $v$, and representation $t_i$, we fit a separate encoding model to predict the BOLD response $\hat{B}$, i.e. $\hat{B}_{(x,v,t_i)} = g_{(x,v,t_i)}(t_i)$. An optimal ridge parameter $\alpha$ was estimated for each $g_{(x,v,t_i)}$ by using 50-fold Monte Carlo cross-validation, with a held-out validation set of 20% of the datapoints from the training dataset. We then measured the encoding model performance $\rho$ by

computing the correlation between the true and predicted BOLD responses for a separate test dataset consisting of one story. That is, $\rho_{(x,v,t_i)}$ measures the capacity of representation $t_i$ to explain the response behavior of voxel $v$ on subject $x$.

#### 4.2.3 Mapping the First Dimension of the Representation Embedding Space to the Brain

If a brain area was specialized for processing a specific type of information, then we would expect representations that capture that information to be good predictors of that brain area. Each voxel in the brain can thus be thought of as another language representation, and we can infer where that representation would lie in the MDS space by projecting it onto those dimensions.

The main MDS dimension (left to right in Figure 2) is especially interesting as it seems to capture an intuitive notion of a language representation hierarchy. Representations with low values along the main dimension include word embeddings as well as the earliest layers of most of the language models and machine translation models. Representations with high values along the main dimension include the deeper layers of these models, as well as the majority of the interpretable syntactic and semantic representations. We tested whether this MDS dimension could capture patterns of hierarchical processing observed in cortex. First we defined $\mathbf{p}_{(x,v)} = \textbf{zscore}([\rho_{(x,v,t_1)} \cdots \rho_{(x,v,t_n)}])$ as the 100-dimensional vector that denotes the encoding model performances for each subject $x$ and voxel $v$, z-scored over all representations $\mathcal{T}$. We then projected each $\mathbf{p}_{(x,v)}$ onto the first MDS dimension by taking their dot product. This gave us a value that quantifies which part of the first MDS dimension best predicts the activity of a given voxel.

Figure 3 shows shows the projection of each voxel for one subject (*lower center*) and averaged across subjects in each anatomical ROI (*upper center*) onto the first MDS dimension. Blue voxels and regions are better predicted by representations that are low on the first MDS dimension, whereas red voxels and regions are better predicted by representations that are high on the first MDS dimension.

While the literature has not settled on a single hierarchical view of language processing in human cortex, one point of general agreement among existing theories is that there is a set of "lower" language areas, including Wernicke's area/auditory cortex (AC), Broca's area (BA), and the premotor speech area sPMv [13, 16]. Across our five subjects, we see negative projections on the first PC (corresponding to earlier LM layers) in AC, but both positive and negative projections in BA and sPMv. This matches other results using narrative stories and encoding models [7] where it was found that, of these three core language areas, AC is the best explained by lower-level features (phonemes and sound spectrum).

Outside of the core language areas, the literature is more divided on representational hierarchy. It is broadly agreed that these other areas constitute the "semantic system" [4] in which language meaning is derived and represented. Our data show that most of these regions have positive projections on the first PC, corresponding to later LM layers. More fine-grained analyses have suggested that some areas, such as the angular gyrus (AG) and precuneus (PrCu), contain the highest-level representations [19, 22]. This neatly matches our results, which show that the angular gyrus and precuneus have the most positive projections on the first PC of any brain areas.

#### 4.2.4 Predicting Encoding Model Performance with Representation Embeddings

If the representation embeddings reflect how the brain represents linguistic information, then it should be possible to match each representation embedding $\mathbf{r}_k$ to its corresponding performance vector $\rho_{(x,\bullet,t_k)}$, which describes how well that representation can predict responses in each cortical voxel. We test this via a leave-two-out experiment, where we train a learner using 98 $(\mathbf{r}_k, \rho_{(x,\bullet,t_k)})$ pairs and then use this learner to predict which of the remaining two representation embeddings match the remaining two performance vectors. If the correlation between the predicted performance vector for representation A matches the ground truth performance vector for representation A better than the ground truth performance vector for representation B (and similarly B matches B better than it matches A), then we have succeeded in correctly discriminating a performance vector from its corresponding representation embedding.

Formally, for each subject $x$ and pair of language representations $(t_i, t_j)$, we trained a linear regression $\hat{h}_{(x,i,j)}$ to map a representation embedding $\mathbf{r}_k$ to the corresponding encoding model performance built from $t_k$ over all voxels.

$$\hat{h}_{(x,t_i,t_j)}(\mathbf{r}_k) \approx corr(g_{(x,\bullet,k)}(t_k), B_{(x,\bullet)}) = \rho_{(x,\bullet,t_k)},$$

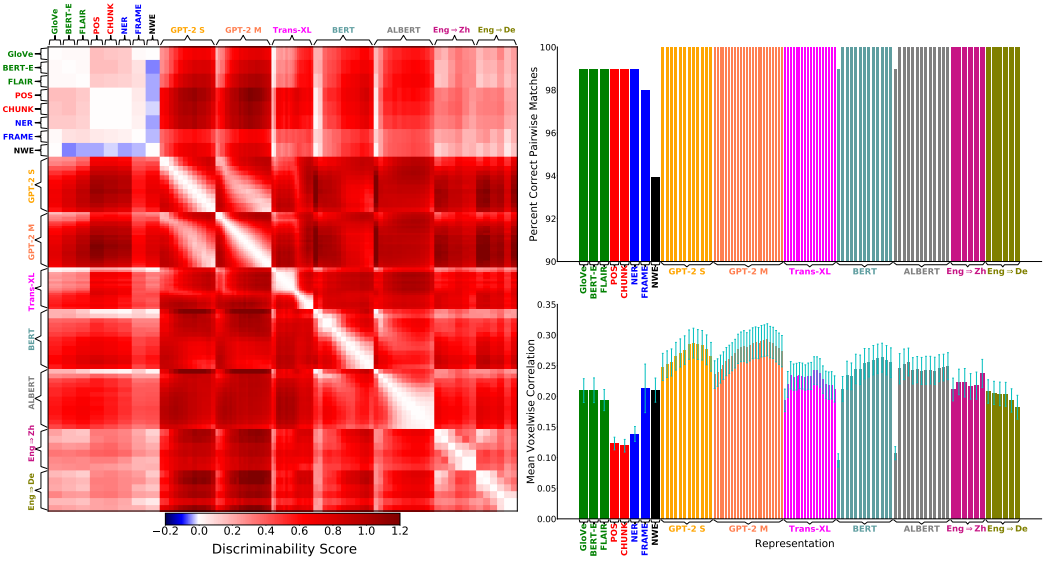


Figure 4: *Representation Embeddings Reflect Brain Responses*: (*Left*): Discriminability score matrix $\mathbf{M}$, the average across each subject matrix $\mathbf{M}_x$, which is computed as described in Section 4.2.4. For each representation, we fit and tested encoding models that predict the fMRI response in each cortical voxel, yielding a pattern of prediction performance across the brain. For each pair, we then tested whether the brain patterns could be correctly matched to the representations on the basis of the representation embeddings shown in Figure 2. Highly discriminable pairs appear red, non-discriminable pairs white, and pairs that are less discriminable than expected by chance appear blue. Most pairs of representations yield brain patterns that are easy to distinguish using the embeddings, suggesting that these embeddings reflect the structure of representations in the human brain. However, some pairs are similar enough in both embedding and brain that discrimination between them falls to chance level, such as the word embeddings (green labels) and nearby layers of language models. (*Upper Right*): The percentage of pairwise matches for each representation where the match is correct more often than not (on 3 or more subjects). Almost all representations can be correctly matched with their corresponding performance vector $\mathbf{p}$, with the interpretable representations being the most difficult to distinguish. (*Lower Right*): Mean voxelwise correlation for encoding models built using each representation of the natural language story stimuli. As seen in other literature [30], the intermediate layers of Transformer-based language models work best as encoding model representations.

$\mathbf{r}_k$ is defined as the 196-element vector that concatenates the row and column that correspond to the representation $t_i$, leaving out the four elements corresponding to the held out pair: $\mathbf{R_{ii}}$, $\mathbf{R_{ij}}$, $\mathbf{R_{ji}}$, and $\mathbf{R_{jj}}$. The model $\hat{h}_{(x,t_i,t_j)}$ was then used to predict the held out encoding model performance across all voxels, $\rho(x, \bullet, t_i)$ and $\rho(x, \bullet, t_j)$. For each subject, we then computed discriminability scores for all pairs of representations to generate a matrix $\mathbf{M}_x$. This quantifies how much better the predicted encoding model performance for $t_i$ matched with the true encoding model performance for $t_i$ than the true encoding model performance for $t_j$ (and vice versa):

$$\begin{aligned}\mathbf{M}_{x_{(i,j)}} =& (corr(\hat{h}_{(x,t_i,t_j)}(\mathbf{r}_i), \rho_{(x,\bullet,t_i)}) + (corr(\hat{h}_{(x,t_i,t_j)}(\mathbf{r}_j), \rho_{(x,\bullet,t_j)}))) \\ &-(corr(\hat{h}_{(x,t_i,t_j)}(\mathbf{r}_i), \rho_{(x,\bullet,t_j)}) + (corr(\hat{h}_{(x,t_i,t_j)}(\mathbf{r}_j), \rho_{(x,\bullet,t_i)})))\end{aligned}$$

Figure 4 shows the discriminability scores for all representation pairs averaged across subjects, as well as the average encoding model performance for each individual representation. The vast majority of pairs have high discriminability scores (*red*), indicating that the representation embeddings broadly capture the structure of the brain's language representations.

However, a few pairs have negative scores (*blue*), indicating below-chance discrimination performance. This could happen by chance, or it could happen if the task affinities are very different from the brain representations. We believe the negative scores for GloVe NWE are caused by the latter. This representation is highly dissimilar from the others, hence its far-removed location in the MDS space. However, the temporal imprecision of the BOLD responses recorded by fMRI (on the order of

1 second, or 2-5 words) renders the GloVe NWE and normal GloVe embeddings nearly identical for predicting brain data. This disconnect is likely the cause of the negative scores.

We also computed how often the discriminability score was higher than 0 in the majority of subjects (at least 3 out of 5). We see (Figure 4, *upper right*) that encoding model performances are well predicted by the representation embeddings, with representation embeddings getting matched to their corresponding encoding model performances over 90% of the time for all representations, and 100% of the time for the majority of representations.

## 5 Future Work, Limitations, and Conclusions

By measuring transferability between different language representations, we were able to visualize the relationships between these representations extracted from common NLP tasks. This uncovered a low-dimensional structure that illustrates how different tasks are related to one another, and how representations evolve over depth in different language models. Finally, we show evidence that these representation embeddings capture the structure of language representations in the human brain.

There are further possible iterations of this method that may shed additional light on the structure of language representations in the brain. Since this method relies on using the transfer properties between representations to generate embeddings, it is necessary that the chosen set of representations spans the rich space of language representations. If some part of the space of language representations has not been sampled, then the representation embeddings may fail to capture some aspects of the structure of that space. We tried to ameliorate this concern by sampling a large number of representations (100). However, it is likely that these chosen representations still do not capture the full diversity of the space. In future work, an even larger number of representations could be used to better map this space.

In a similar vein, we also represented the input to our encoder-decoder setup as a "universal" representation, for which we decided to use GloVe embeddings. GloVe embeddings are likely not "universal" in a true sense, in the same way that a one-hot encoding of the story might be, but practical concerns made this approximation necessary. Use of other universal spaces could also be enlightening, such as directly using fMRI data to map to a latent representation space – i.e. replace $U(S)$ in Figure 1 with some fMRI BOLD responses $B$ recorded from the same language comprehension experiment. Of course the possibilities are not restricted to language representations, as previous work had focused on vision instead [39, 44].

We also used linear as opposed to nonlinear networks for our encoder-decoders. This limits the expressiveness of the transfer networks, and thus may under-estimate the relatedness between tasks. However, using only linear networks also increases interpretability by ensuring that only simply-related representations can transfer to one another, as also noted by others [2, 26]. Future work may explore the use of regularized nonlinear models for the encoder-decoder networks.

This method does require extracting representations from a neural network trained to accomplish some task. For many tasks used in linguistics, neuroscience, and cognitive psychology, there is no existing pre-trained network. However, training artificial neural networks on a task that is used to measure cognition in humans and animals is an emerging method that can shed light on how these tasks are accomplished [11, 35, 42], and provide standardized benchmarks for comparing between different computational cognitive models. Furthermore, we can use our proposed method to understand what representations are needed to accomplish different tasks, and to visualize the relationships between those representations. For example, the debate on whether lexico-semantic and syntactic representations are actually separable [14] centers on evidence from different tasks that claim to measure syntactic representations versus semantic ones. The claims about the tasks themselves are difficult to test – but methods like those presented in this work can directly quantify how much information is shared between representations needed to accomplish those tasks, either in artificial neural networks or in neuroimaging data. Our proposed method may even provide new evidence in other domains where overlap has been observed between neural representations elicited by ostensibly different cognitive tasks [3, 38].

In sum, we believe that our work can provide a template for investigating relationships between linguistic and cognitive representations in many different domains.

## Acknowledgements

We would like to thank Amanda LeBel for collecting the fMRI data and reconstructing cortical surfaces, Lauren Wagner for annotating the experimental stimuli, and the anonymous reviewers for their insights and suggestions. Funding for this work was provided by the Burroughs-Wellcome Fund Career Award at the Scientific Interface (CASI), Intel Corporation, the Whitehall Foundation, and the Alfred P. Sloan Foundation. The authors declare no conflict-of-interest.

## References

[1] Alan Akbik, Tanja Bergmann, Duncan Blythe, Kashif Rasul, Stefan Schweter, and Roland Vollgraf. Flair: An easy-to-use framework for state-of-the-art nlp. In *Proceedings of the 2019 Conference of the North American Chapter of the Association for Computational Linguistics (Demonstrations)*, pages 54–59, 2019.

[2] Guillaume Alain and Yoshua Bengio. Understanding intermediate layers using linear classifier probes. *arXiv preprint arXiv:1610.01644*, 2016.

[3] Edward Awh and John Jonides. Overlapping mechanisms of attention and spatial working memory. *Trends in Cognitive Sciences*, 5(3):119–126, Mar 2001. ISSN 1364-6613. doi: 10.1016/S1364-6613(00)01593-X.

[4] Jeffrey R Binder, Rutvik H Desai, William W Graves, and Lisa L Conant. Where is the semantic system? a critical review and meta-analysis of 120 functional neuroimaging studies. *Cerebral cortex*, 19(12):2767–2796, 2009.

[5] Charlotte Caucheteux and Jean-Rémi King. Language processing in brains and deep neural networks: computational convergence and its limits. *bioRxiv*, 2020. doi: 10.1101/2020.07.03.186288. URL `https://www.biorxiv.org/content/early/2020/07/04/2020.07.03.186288`.

[6] Zihang Dai, Zhilin Yang, Yiming Yang, William W Cohen, Jaime Carbonell, Quoc V Le, and Ruslan Salakhutdinov. Transformer-xl: Attentive language models beyond a fixed-length context. *arXiv preprint arXiv:1901.02860*, 2019.

[7] Wendy A de Heer, Alexander G Huth, Thomas L Griffiths, Jack L Gallant, and Frédéric E Theunissen. The hierarchical cortical organization of human speech processing. *Journal of Neuroscience*, 37(27):6539–6557, 2017.

[8] Scott Deerwester, Susan T Dumais, George W Furnas, Thomas K Landauer, and Richard Harshman. Indexing by latent semantic analysis. *Journal of the American society for information science*, 41(6):391–407, 1990.

[9] Christophe Destrieux, Bruce Fischl, Anders Dale, and Eric Halgren. Automatic parcellation of human cortical gyri and sulci using standard anatomical nomenclature. *Neuroimage*, 53(1): 1–15, 2010.

[10] Jacob Devlin, Ming-Wei Chang, Kenton Lee, and Kristina Toutanova. Bert: Pre-training of deep bidirectional transformers for language understanding. In *Proceedings of the 2019 Conference of the North American Chapter of the Association for Computational Linguistics: Human Language Technologies, Volume 1 (Long and Short Papers)*, pages 4171–4186, 2019.

[11] Daniel B. Ehrlich, Jasmine T. Stone, David Brandfonbrener, Alexander Atanasov, and John D. Murray. Psychrnn: An accessible and flexible python package for training recurrent neural network models on cognitive tasks. *eNeuro*, 8(1), Jan 2021. ISSN 2373-2822. doi: 10.1523/ENEURO.0427-20.2020. URL `https://www.eneuro.org/content/8/1/ENEURO.0427-20.2020`.

[12] Kawin Ethayarajh. How contextual are contextualized word representations? comparing the geometry of bert, elmo, and gpt-2 embeddings. *arXiv preprint arXiv:1909.00512*, 2019.

[13] Evelina Fedorenko, John Duncan, and Nancy Kanwisher. Language-selective and domain-general regions lie side by side within broca's area. *Current Biology*, 22(21):2059–2062, 2012.

[14] Evelina Fedorenko, Idan Asher Blank, Matthew Siegelman, and Zachary Mineroff. Lack of selectivity for syntax relative to word meanings throughout the language network. *Cognition*, 203, Oct 2020. ISSN 0010-0277. doi: 10.1016/j.cognition.2020.104348.

[15] Bruce Fischl. Freesurfer. *Neuroimage*, 62(2):774–781, 2012.

[16] Gregory Hickok and David Poeppel. The cortical organization of speech processing. *Nature reviews neuroscience*, 8(5):393–402, 2007.

[17] Alexander G Huth, Wendy A De Heer, Thomas L Griffiths, Frédéric E Theunissen, and Jack L Gallant. Natural speech reveals the semantic maps that tile human cerebral cortex. *Nature*, 532 (7600):453–458, 2016.

[18] Shailee Jain and Alexander Huth. Incorporating context into language encoding models for fmri. In S. Bengio, H. Wallach, H. Larochelle, K. Grauman, N. Cesa-Bianchi, and R. Garnett, editors, *Advances in Neural Information Processing Systems*, volume 31. Curran Associates, Inc., 2018. URL `https://proceedings.neurips.cc/paper/2018/file/f471223d1a1614b58a7dc45c9d01df19-Paper.pdf`.

[19] Shailee Jain, Vy Vo, Shivangi Mahto, Amanda LeBel, Javier S Turek, and Alexander Huth. Interpretable multi-timescale models for predicting fmri responses to continuous natural speech. In H. Larochelle, M. Ranzato, R. Hadsell, M. F. Balcan, and H. Lin, editors, *Advances in Neural Information Processing Systems*, volume 33, pages 13738–13749. Curran Associates, Inc., 2020. URL `https://proceedings.neurips.cc/paper/2020/file/9e9a30b74c49d07d8150c8c83b1ccf07-Paper.pdf`.

[20] Simon Kornblith, Mohammad Norouzi, Honglak Lee, and Geoffrey Hinton. Similarity of neural network representations revisited. In *International Conference on Machine Learning*, pages 3519–3529. PMLR, 2019.

[21] Zhenzhong Lan, Mingda Chen, Sebastian Goodman, Kevin Gimpel, Piyush Sharma, and Radu Soricut. Albert: A lite bert for self-supervised learning of language representations. *arXiv preprint arXiv:1909.11942*, 2019.

[22] Yulia Lerner, Christopher J Honey, Lauren J Silbert, and Uri Hasson. Topographic mapping of a hierarchy of temporal receptive windows using a narrated story. *Journal of Neuroscience*, 31 (8):2906–2915, 2011.

[23] Shinji Nishimoto, An T Vu, Thomas Naselaris, Yuval Benjamini, Bin Yu, and Jack L Gallant. Reconstructing visual experiences from brain activity evoked by natural movies. *Current biology*, 21(19):1641–1646, 2011.

[24] Shinji Nishimoto, Alexander G Huth, Natalia Y Bilenko, and Jack L Gallant. Eye movement-invariant representations in the human visual system. *Journal of vision*, 17(1):11–11, 2017.

[25] Jeffrey Pennington, Richard Socher, and Christopher Manning. Glove: Global vectors for word representation. In *Proceedings of the 2014 conference on empirical methods in natural language processing (EMNLP)*, pages 1532–1543, 2014.

[26] Tiago Pimentel, Josef Valvoda, Rowan Hall Maudslay, Ran Zmigrod, Adina Williams, and Ryan Cotterell. Information-theoretic probing for linguistic structure. In *Proceedings of the 58th Annual Meeting of the Association for Computational Linguistics*, pages 4609–4622, 2020.

[27] Alec Radford, Jeffrey Wu, Rewon Child, David Luan, Dario Amodei, and Ilya Sutskever. Language models are unsupervised multitask learners. *OpenAI Blog*, 1(8), 2019.

[28] R.W. Saaty. The analytic hierarchy process—what it is and how it is used. *Mathematical Modelling*, 9(3):161–176, 1987. ISSN 0270-0255. doi: https://doi.org/10.1016/0270-0255(87)90473-8. URL `https://www.sciencedirect.com/science/article/pii/0270025587904738`.

[29] Helmut Schmid. Part-of-speech tagging with neural networks. *arXiv preprint cmp-lg/9410018*, 1994.

[30] Martin Schrimpf, Idan Blank, Greta Tuckute, Carina Kauf, Eghbal A. Hosseini, Nancy Kanwisher, Joshua Tenenbaum, and Evelina Fedorenko. The neural architecture of language: Integrative reverse-engineering converges on a model for predictive processing. *bioRxiv*, 2020. doi: 10.1101/2020.06.26.174482. URL https://www.biorxiv.org/content/early/2020/10/09/2020.06.26.174482.

[31] Youwei Song, Jiahai Wang, Zhiwei Liang, Zhiyue Liu, and Tao Jiang. Utilizing bert intermediate layers for aspect based sentiment analysis and natural language inference. *arXiv preprint arXiv:2002.04815*, 2020.

[32] Jörg Tiedemann and Santhosh Thottingal. OPUS-MT — Building open translation services for the World. In *Proceedings of the 22nd Annual Conferenec of the European Association for Machine Translation (EAMT)*, Lisbon, Portugal, 2020.

[33] Mariya Toneva and Leila Wehbe. Interpreting and improving natural-language processing (in machines) with natural language-processing (in the brain). In H. Wallach, H. Larochelle, A. Beygelzimer, F. d'Alché-Buc, E. Fox, and R. Garnett, editors, *Advances in Neural Information Processing Systems*, volume 32. Curran Associates, Inc., 2019. URL https://proceedings.neurips.cc/paper/2019/file/749a8e6c231831ef7756db230b4359c8-Paper.pdf.

[34] Warren S Torgerson. Multidimensional scaling: I. theory and method. *Psychometrika*, 17(4): 401–419, 1952.

[35] Ben Tsuda, Kay M. Tye, Hava T. Siegelmann, and Terrence J. Sejnowski. A modeling framework for adaptive lifelong learning with transfer and savings through gating in the prefrontal cortex. *Proceedings of the National Academy of Sciences*, 117(47):29872–29882, Nov 2020. ISSN 0027-8424, 1091-6490. doi: 10.1073/pnas.2009591117.

[36] https://themoth.org. The moth radio hour, 2020.

[37] Tu Vu, Tong Wang, Tsendsuren Munkhdalai, Alessandro Sordoni, Adam Trischler, Andrew Mattarella-Micke, Subhransu Maji, and Mohit Iyyer. Exploring and predicting transferability across NLP tasks. In *Proceedings of the 2020 Conference on Empirical Methods in Natural Language Processing (EMNLP)*, pages 7882–7926, Online, November 2020. Association for Computational Linguistics. doi: 10.18653/v1/2020.emnlp-main.635. URL https://www.aclweb.org/anthology/2020.emnlp-main.635.

[38] Vincent Walsh. A theory of magnitude: common cortical metrics of time, space and quantity. *Trends in Cognitive Sciences*, 7(11):483–488, Nov 2003. ISSN 1364-6613. doi: 10.1016/j.tics.2003.09.002.

[39] Aria Wang, Michael Tarr, and Leila Wehbe. Neural taskonomy: Inferring the similarity of task-derived representations from brain activity. In H. Wallach, H. Larochelle, A. Beygelzimer, F. d'Alché-Buc, E. Fox, and R. Garnett, editors, *Advances in Neural Information Processing Systems*, volume 32. Curran Associates, Inc., 2019. URL https://proceedings.neurips.cc/paper/2019/file/f490c742cd8318b8ee6dca10af2a163f-Paper.pdf.

[40] Leila Wehbe, Brian Murphy, Partha Talukdar, Alona Fyshe, Aaditya Ramdas, and Tom Mitchell. Simultaneously uncovering the patterns of brain regions involved in different story reading subprocesses. *PloS one*, 9(11):e112575, 2014.

[41] Thomas Wolf, Lysandre Debut, Victor Sanh, Julien Chaumond, Clement Delangue, Anthony Moi, Pierric Cistac, Tim Rault, R'emi Louf, Morgan Funtowicz, and Jamie Brew. Huggingface's transformers: State-of-the-art natural language processing. *ArXiv*, abs/1910.03771, 2019.

[42] Guangyu Robert Yang, Madhura R. Joglekar, H. Francis Song, William T. Newsome, and Xiao-Jing Wang. Task representations in neural networks trained to perform many cognitive tasks. *Nature Neuroscience*, 22(2), Feb 2019. ISSN 1546-1726. doi: 10.1038/s41593-018-0310-2.

[43] An Gie Yong, Sean Pearce, et al. A beginner's guide to factor analysis: Focusing on exploratory factor analysis. *Tutorials in quantitative methods for psychology*, 9(2):79–94, 2013.

[44] Amir R. Zamir, Alexander Sax, William Shen, Leonidas J. Guibas, Jitendra Malik, and Silvio Savarese. Taskonomy: Disentangling task transfer learning. In *Proceedings of the IEEE Conference on Computer Vision and Pattern Recognition (CVPR)*, June 2018.

## A Representation Descriptions

**GloVE** [25] is a 300-dimensional word embedding space. It is an dimensionality-representation representation of word-word co-occurrence statistics. GloVe embeddings were sourced from `http://nlp.stanford.edu/data/glove.6B.zip`

**BERT-E** [10] is a 3072-dimensional contextualized word embedding space extracted from BERT. We used the Flair NLP [1] implementation of BERT embeddings.

**FLAIR** [1] is a 4096-dimensional contextualized character level word embedding space. We used the Flair NLP implementation of this word embedding space.

**POS** is the 53-dimensional representation stored at the pre-softmaxed output logit layer of the pre-trained FLAIR [1] part-of-speech LSTM-based sentence tagger.

**CHUNK** is the 45-dimensional representation stored at the pre-softmaxed output logit layer of the pre-trained FLAIR [1] LSTM-based sentence chunker.

**NER** is the 76-dimensional representation stored at the pre-softmaxed output logit layer of the pre-trained FLAIR [1] LSTM-based named entity recognition sentence tagger.

**FRAME** is the 5196-dimensional representation stored at the pre-softmaxed output logit layer of the pre-trained FLAIR [1] LSTM-based semantic framing (verb disambiguation) tagger.

**NWE** is the **GloVe** representation, offset by one word in the future.

The FlairNLP repository which we used for the preceding represenations can be found here: `https://github.com/flairNLP/`

**GPT-2 Small** is a set of 12 representations, each 768-dimensional, built from each hidden state output from the 12 transformers that compose the GPT-2 Small unidirectional language model [27]. Representations were built using a sliding window of 64 words as a context. We used the HuggingFace [41] implementation of this network to extract feature for these representations.

**GPT-2 Medium** is a set of 24 representations, each 1024-dimensional, built from each hidden state output from the 24 transformers that compose the GPT-2 Medium unidirectional language model [27]. Representations were built using a sliding window of 64 words as a context. We used the HuggingFace [41] implementation of this network to extract feature for these representations.

**Transformer-XL** is a set of 18 representations, each 1024-dimensional, built from each hidden state output from the 18 transformers that compose the Transformer-XL unidirectional language model [6]. Representations were built using a sliding window of 64 words as a context. We used the HuggingFace [41] implementation of this network to extract feature for these representations.

**BERT** is a set of 13 representations, each 768-dimensional, built from the encoded input and each hidden state output from the 12 transformers that compose the BERT bidirectional masked language model [10]. Representations were built using a sliding window of 64 words as a context, with the last token being the designated mask token. We used the HuggingFace [41] implementation of this network to extract feature for these representations.

**ALBERT** is a set of 13 representations, each 768-dimensional, built from the encoded input and each hidden state output from the 12 transformers that compose the ALBERT bidirectional masked language model [21]. Representations were built using a sliding window of 64 words as a context, with the last token being the designated mask token. We used the HuggingFace [41] implementation of this network to extract feature for these representations.

**Eng** $\Rightarrow$ **Zh** is the set of 6 encoder hidden state representations, each 512-dimensional, of the HuggingFace/Helsinki-NLP [41, 32] implementation of a Transformer-based machine translation model from English to Mandarin Chinese. Representations were built using a sliding window of 64 words as a context. The pretrained network we used can be found here: `https://huggingface.co/Helsinki-NLP/opus-mt-en-zh`.

**Eng** $\Rightarrow$ **De** is the set of 6 encoder hidden state representations, each 512-dimensional, of the HuggingFace/Helsinki-NLP [41, 32] implementation of a Transformer-based machine translation model from English to German. Representations were built using a sliding window of 64 words as a context. The pretrained network we used can be found here: `https://huggingface.co/Helsinki-NLP/opus-mt-en-de`.

Table 1: Stories used for stimuli for fMRI scanning

| Story | Use | Words | TRs |
|---|---|---|---|
| Alternate Ithaca Tom | Train | 2174 | 343 |
| Saving Souls | Train | 1868 | 355 |
| Avatar | Train | 1469 | 367 |
| Legacy | Train | 1893 | 400 |
| Ode to Stepfather | Train | 2675 | 404 |
| Under the Influence | Train | 1641 | 304 |
| How to Draw a Naked Man | Train | 1964 | 354 |
| Naked | Train | 3218 | 422 |
| Life Flight | Train | 2209 | 430 |
| Stage Fright | Train | 2067 | 293 |
| Till Death or Homosexuality Do Us Part | Train | 2297 | 323 |
| From Boyhood to Fatherhood | Train | 2755 | 348 |
| Sloth | Train | 2403 | 437 |
| Exorcism | Train | 2949 | 467 |
| Have You Met Him Yet | Train | 2985 | 496 |
| A Doll's House | Train | 1656 | 241 |
| The Closet that Ate Everything | Train | 1928 | 314 |
| Adventures in Saying Yes | Train | 2309 | 391 |
| Buck | Train | 1677 | 332 |
| Swimming With Astronauts | Train | 2127 | 385 |
| That Thing on My Arm | Train | 2336 | 434 |
| Eye Spy | Train | 2127 | 379 |
| It's a Box | Train | 2336 | 355 |
| Hangtime | Train | 1708 | 324 |
| Where There's Smoke | Test | 1839 | 291 |

# B fMRI Data Details

## B.1 Stimulus details.

Training stimuli for encoding models consisted of stories from *The Moth Radio Hour*: "Alternate Ithaca Tom", "Saving Souls", "Avatar", "Legacy", "Ode to Stepfather", "Under the Influence", "How to Draw a Naked Man", "Naked", "Life Flight", "Stage Fright", "Till Death or Homosexuality Do Us Part", "From Boyhood to Fatherhood", "Sloth", "Exorcism", "Have You Met Him Yet", "A Doll's House", "The Closet that Ate Everything", "Adventures in Saying Yes", "Buck", "Swimming With Astronauts", "That Thing on My Arm", "Eye Spy", "It's a Box", and "Hangtime".

The test stimulus was a single story, also taken from *The Moth Radio Hour*: "Where There's Smoke". The amount of data in terms of words and TRs from each story is given in Table 1.

## B.2 ROI labels

Regions of interest (ROIs) were labelled in each subject using separate localizer data, as follows:

The auditory cortex (AC) was selected as a region with highly repeatably responses to ten presentations of a one-minute stimulus consisting of music, speech, and natural environmental sounds.

Visual category-selective areas were defined using a category localizer where subjects looked at a series of images while fixating on the center of the screen. Place-selective visual areas, including the retrosplenial complex (RSC), occipital place area (OPA, called TOS for trans-occipital sulcus in some subjects), and parahippocampal place area (PPA), were defined by contrasting responses to place images (e.g. buildings) with responses to object images (e.g. teapots). Face-selective visual areas, including the fusiform face area (FFA), occipital face area (OFA), and inferior frontal sulcus face patch (IFSFP) were defined by contrasting responses to face images with responses to object images. Body-selective visual areas, including the extrastriate body area (EBA) and fusiform body area (FBA) were defined by contrasting responses to body images with responses to object images.

Motor-related areas were defined using a ten-minute motor localizer in which subjects were asked to wiggle their fingers, wiggle their toes, mouth nonsense syllables (e.g. *balabalabala*), make saccades, or silently generate speech. Eye movement areas, including the frontal eye fields (FEF), intraparietal sulcus (IPS), fronto-opercular eye movement area (FO), and supplementary eye fields (SEF) were defined by contrasting the eye movement condition with rest. Hand areas, including primary somatomotor hand cortex (M1H, S1H), ventral premotor hand area (PMvh), secondary somatosensory hand area (S2H), and supplementary motor hand area (SMHA) were defined by contrasting the hand movement condition with rest. Foot areas, including primary somatomotor foot cortex (M1F, S1F), supplementary motor foot area (SMFA), and secondary somatosensory foot area (S2F) were defined by contrasting the foot movement condition with rest. Mouth movement areas, including primary somatomotor mouth cortex (M1M, S1M) and secondary somatosensory mouth cortex (S2M) were defined by contrasting the mouth movement condition with rest. Speech areas, including Broca's area (Broca) and the superior ventral premotor speech area (sPMv) were defined by contrasting the silent language generation condition with rest.

In some subjects, retinotopic areas (V1-V4, LO, V7, V3A, V3B) were defined using standard retinotopic mapping protocols.

In some subjects, the human analogue of the middle temporal visual motion area (hMT or MT) was defined using a contrast of coherently moving visual dots versus randomly flickering visual dots.

## C fMRI Encoding Performance Similarity Matrix

A similarity matrix showing the correlations between the performance vectors for each pair of representations is given below. This can be compared to the dicriminablity matrix in Figure 4 as a ground truth metric of the the difficulty of comparing two encoding models if the representation embeddings perfectly captured all of the differences across representations. This suggests that the representation embeddings are better at capturing certain kinds of differences between representations, such as the differences across layers of the same network.

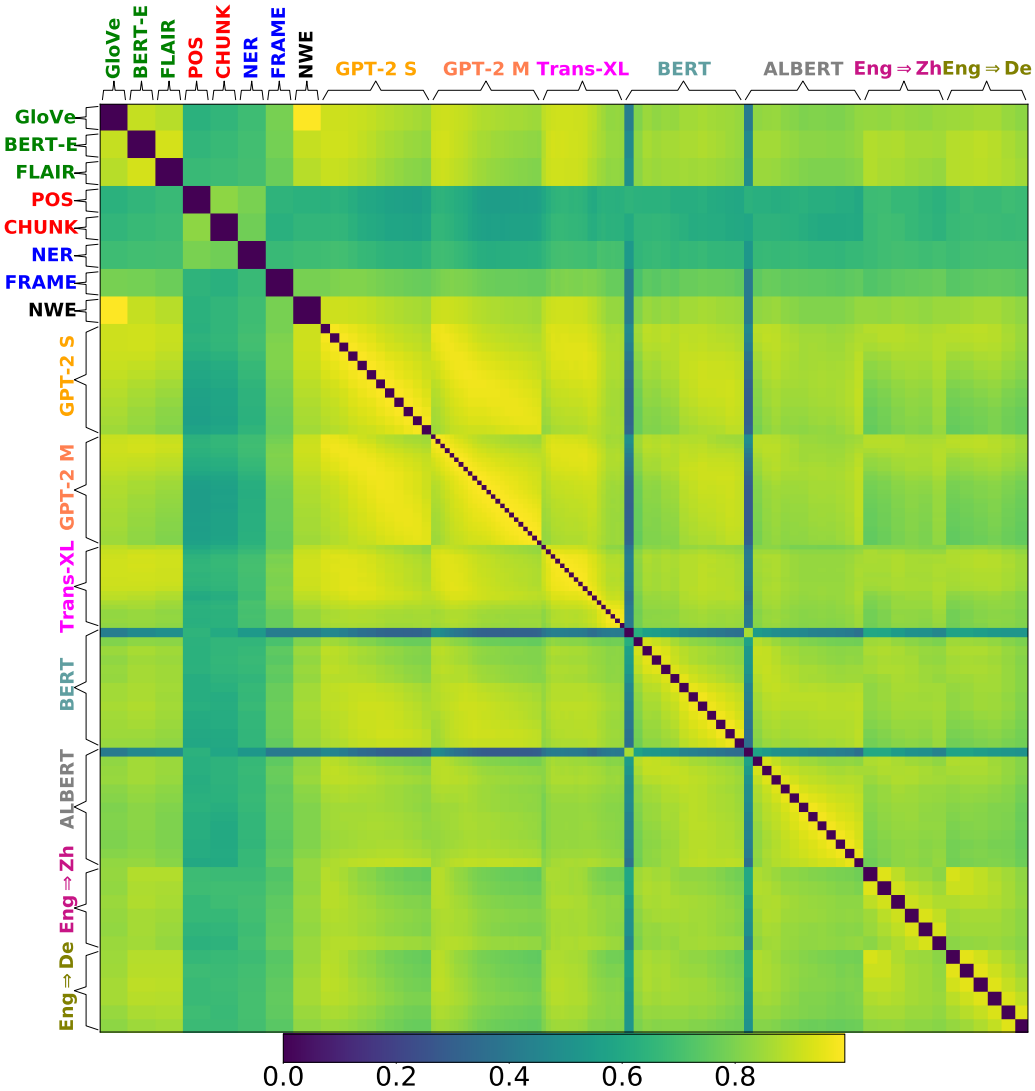
GloVe
BERT-E
FLAIR
POS
CHUNK
NER
FRAME
NWE
GPT-2 S
GPT-2 M
Trans-XL
BERT
ALBERT
Eng ⇒ Zh
Eng ⇒ De
0.0
0.2
0.4
0.6
0.8

# D Embedding Brain Voxels in the MDS Space

## D.1 Other Subjects

A 3D visualization of a single subject's brain voxels embedded into the first main MDS dimension was presented in Figure 3. Flatmaps showing the same metric the other four subjects are shown below. Scales have been adjusted on a per-subject basis to maximize visual contrast.

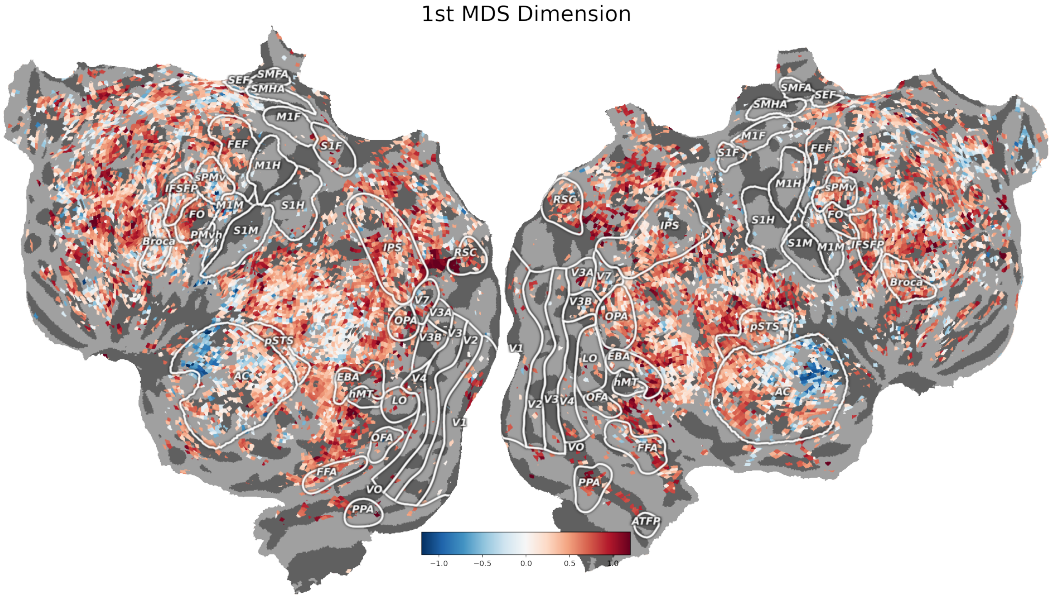


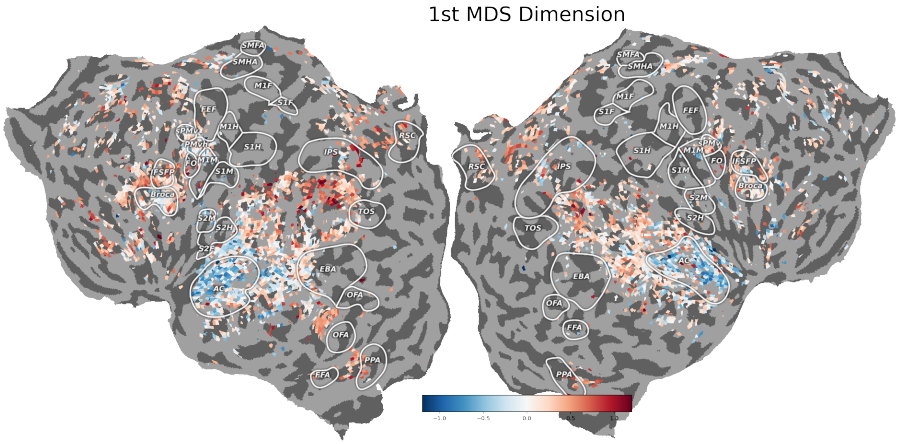

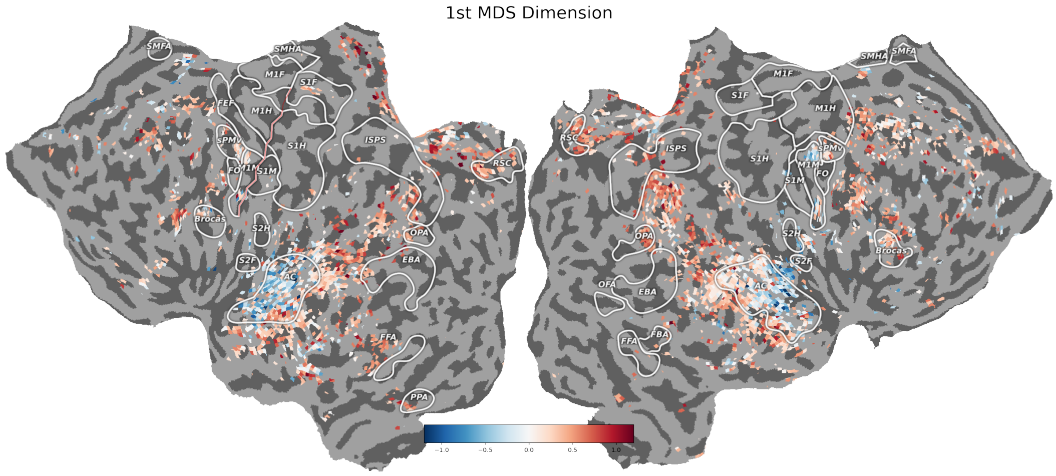
1st MDS Dimension
SMFA
SMHA
M1F
S1F
FEF
M1H
PMV
S1H
ISPS
RSC
FO
M1M
S1M
Broca's
S2H
OPA
S2F
EBA
AC
FFA
PPA
OFA
FBA
−1.0
−0.5
0.0
0.5
1.0

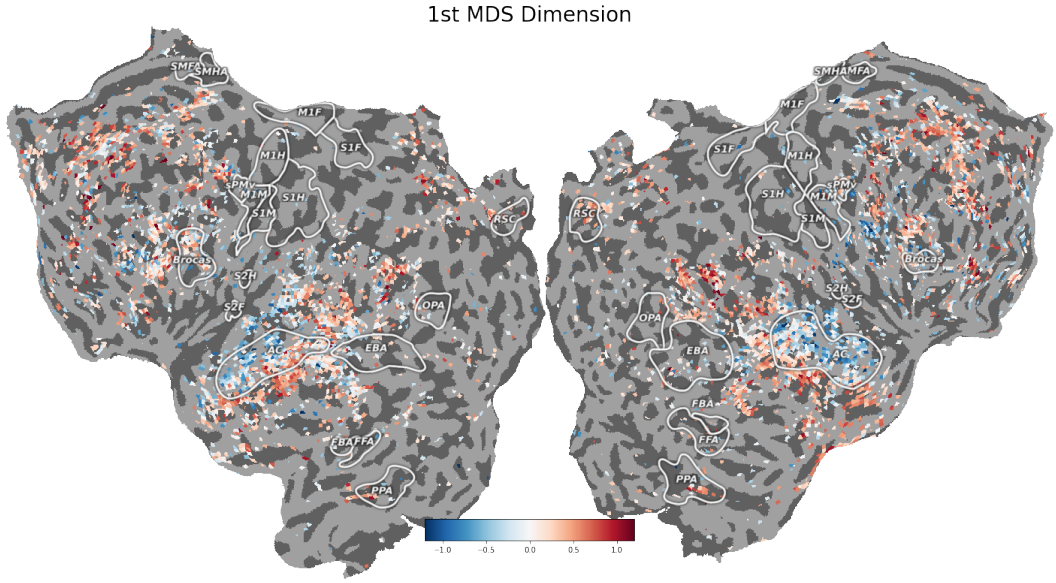
1st MDS Dimension
SMFA
SMHA
M1F
S1F
M1H
PMV
M1M
S1H
S1M
RSC
Broca's
S2H
S2F
OPA
AC
EBA
FBA
FFA
PPA
−1.0
−0.5
0.0
0.5
1.0

### D.2 Anatomical ROI Projection in the MDS Space

The numerical projections of the anatomical ROIs from Figure 3 are shown below. ROIs are labeled as in the Destrieux 2009 atlas [9].

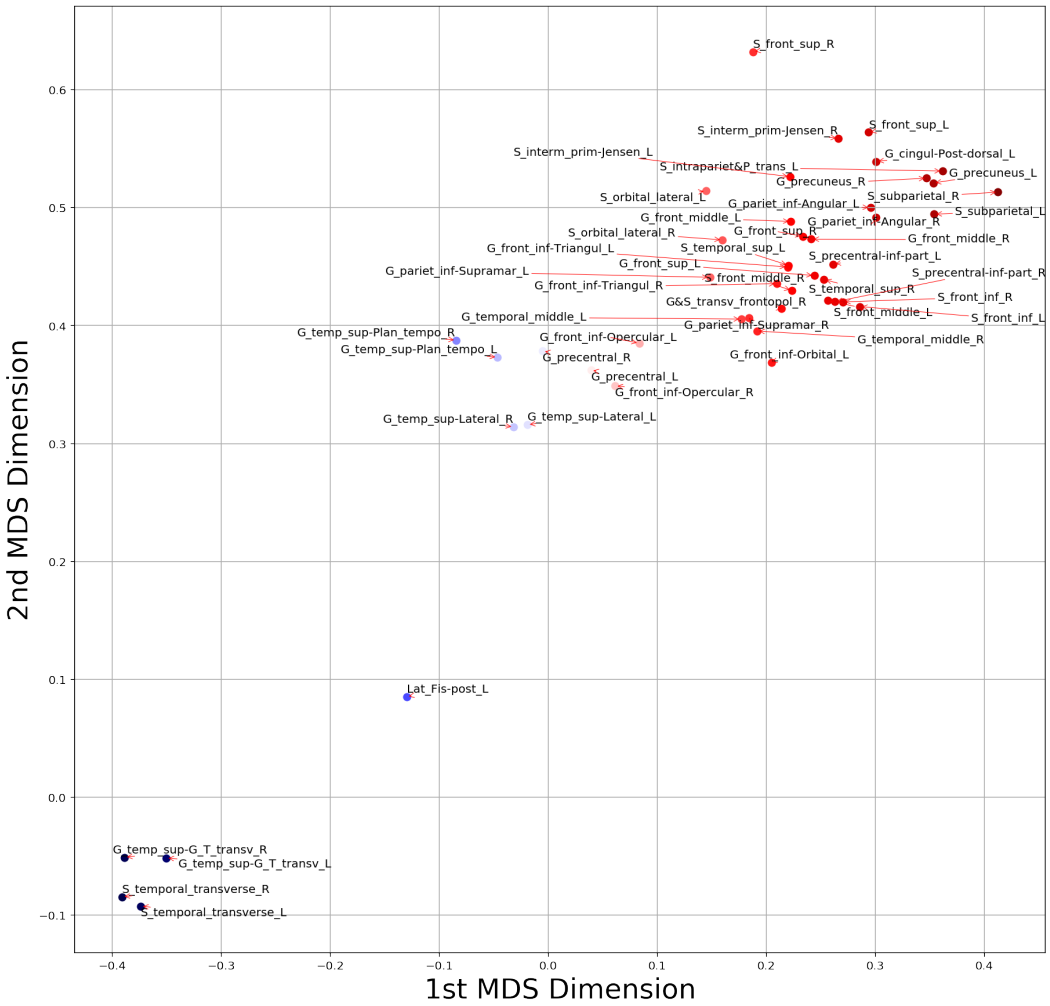


## E Experimental Setup Details

The encoder-decoder setup (before replacing decoders) was initially trained using batches of size 1024 using stochastic gradient descent using a nonstandard negative correlation coefficient loss function. We found empirically that this setup provided faster convergence and good compression into the latent spaces as it was scale-invariant to the different dimensions in the various representations. The decoders were then trained on a standard mean squared error loss after they were replaced and retrained. When decoders were retrained, *all* decoders were retrained, including decoders to the same task (e.g. $D_{t_1 \to t_1}$). This was to ensure that pairwise comparisons across decoders was performed with a consistent methodology between all pairs. Hyperparameter values were chosen via coordinate descent over a small set of values: $(10, 20, 50)$ for the latent state dimensionality, $(10^{-6}, 2 \times 10^{-5}, 10^{-4}, 2 \times 10^{-4}, 10^{-4})$ for the learning rates, for each of the encoder and decoder halves of the training, and $(256, 512, 1024)$ for batch size. Overall results did not vary significantly with latent space dimensionality. Training was done using an early stopping criterion of 1000 batches or the first batch where loss failed to improve, whichever came first. Scripts for the experimental setup have been included in the supplementary material.

## F Details on the Generation of the Pairwise Tournament Matrix $\mathbf{W}$ and Representation Embedding Matrix $\mathbf{R}$

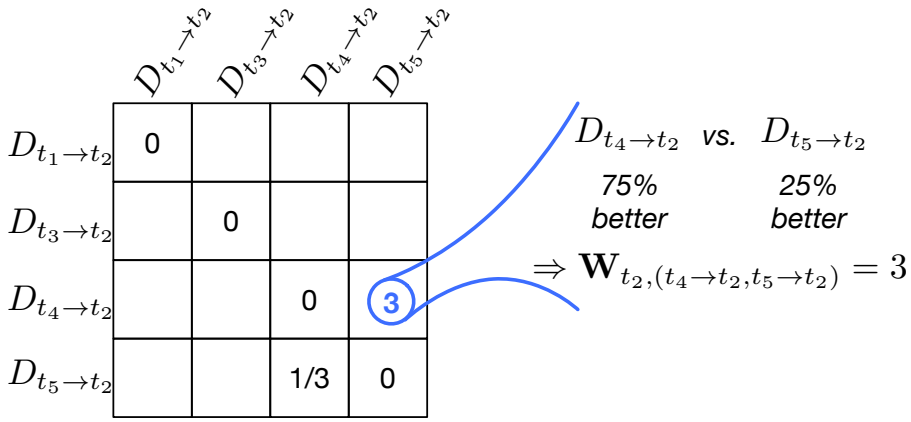


Figure 5: *Generation and Use of the Pairwise Tournament Matrix* $\mathbf{W}$*:* The decoders from a given latent space are compared in the generation of the pairwise tournament matrix for task $t_2$ $\mathbf{W_{t_2}}$. The proportion of the data for which each decoder outperforms the other is measured and compared. Diagonals of this matrix are set to 0. The eigenvector of this matrix with the highest eigenvalue is then assigned to be the row of our representation embedding matrix $\mathbf{R}$ corresponding to that matrix's encoded task. Eigenvectors and eigenvalues are computed using the differential quotient-difference algorithm. Complex components of the eigenvalue are ignored.

## G Visual Aid Reproductions

The matrices from Figure 2 and Figure 4 are very dense. As a visual aid, these matrices have been reproduced here at a larger scale.

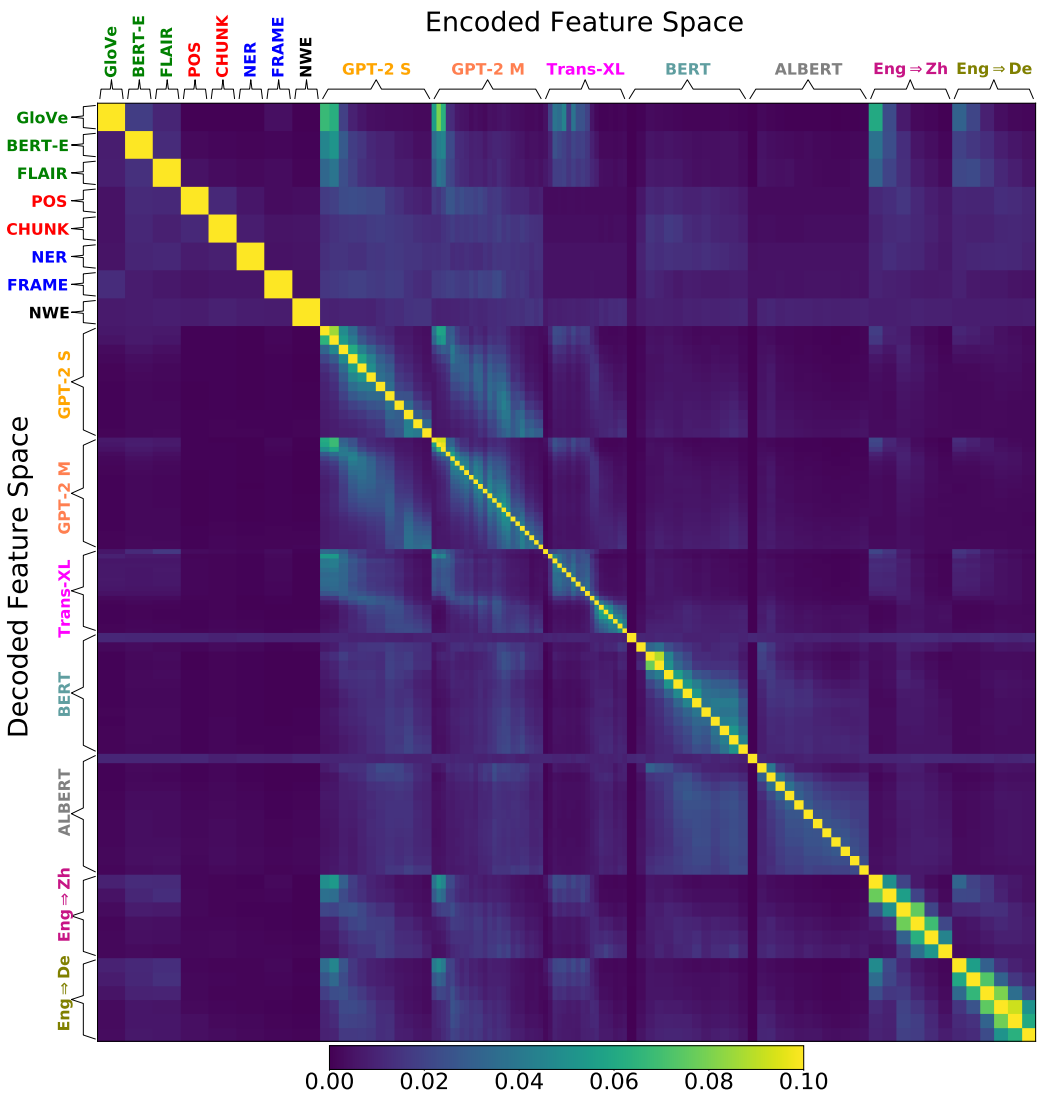

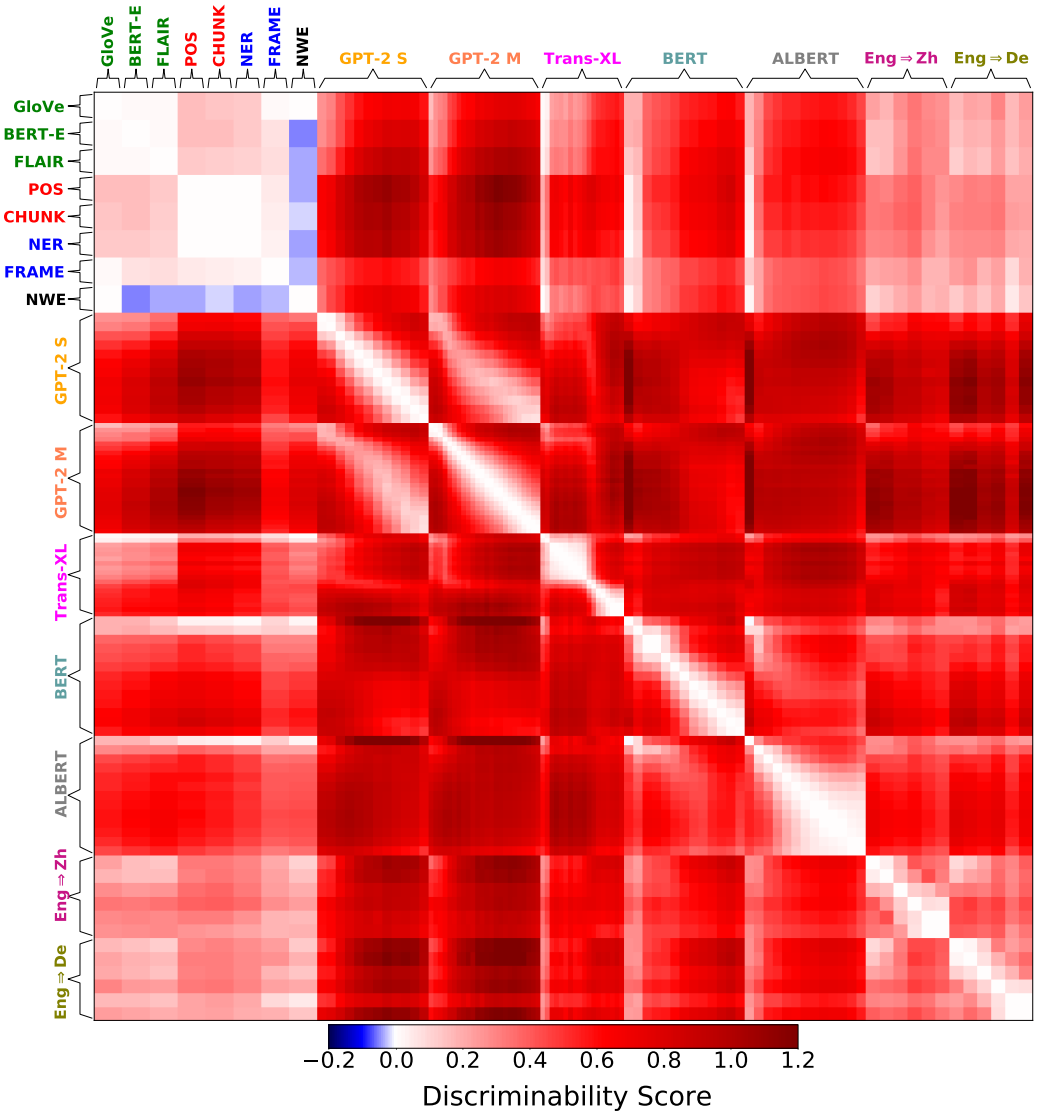
GloVe
BERT-E
FLAIR
POS
CHUNK
NER
FRAME
NWE
GPT-2 S
GPT-2 M
Trans-XL
BERT
ALBERT
Eng ⇒ Zh
Eng ⇒ De
−0.2
0.0
0.2
0.4
0.6
0.8
1.0
1.2
Discriminability Score